Thomas double scattering in electron capture from oriented molecular hydrogen

Steven Alston
Physics Department, Pennsylvania State University, Wilkes-Barre Campus, Lehman, Pennsylvania 18627 and Theoretical Physics, University of Tennessee, Knoxville, Tennessee 37996*

Thomas Brennan† and Frank Bannon III‡
Physics Department, Pennsylvania State University, Wilkes-Barre Campus, Lehman, Pennsylvania 18627
(Received 16 December 1994)

Electron capture from hydrogen molecules by protons is treated using the second-order Born approximation. Differential cross sections in the fixed-nuclei approximation for specific molecular orientations and for an equally weighted averaging over all orientations are presented for incident energies of 2.5 and 10 MeV. A Hartree-Fock molecular wave function and linearized-propagator approximation are employed to evaluate the amplitude. An approximate factoring of the amplitude into double scattering and diffraction (arising from the two target nuclei) components is shown to give a poor description of high-velocity molecular capture.

PACS number(s): 34.70.+e, 34.90.+q, 34.50.Gb, 82.30.Fi

I. INTRODUCTION

The double-scattering mechanism of high-velocity electron capture from atoms has been much studied [1–6]. The Thomas peak in the differential cross section, located at a scattering angle of 0.47 mrad for incident protons, is the signature of this two-step process where the electron scatters first off the projectile and then off the target ion, both collisions occurring at $\sim 60°$. When the target particle is a molecule, the possibility arises of interference occurring between the (second) scattering of the electron off either of the molecular nuclei. Since the first collision is with the projectile, the peak location is not altered when the target is a molecule; however, the peak shape and height may be. Study of the double-scattering mechanism in ion-molecule collisions is of particular interest because the prominent signature of the mechanism in the cross section allows the interplay of the mechanism with the diffraction aspect to be more cleanly investigated.

The second-order Born (B2) approximation to the exact electron capture amplitude is applied to collisions of protons on hydrogen molecules [7]. The B2 amplitude is known to represent the double-scattering mechanism quantum mechanically to lowest order [2]. A Hartree-Fock wave function (HF) giving a good molecular energy and equilibrium separation [8] and a screened electron–molecular-core (two-center) potential derived from it are employed. Comparison is made with a single-ζ molecular-orbital model. The free propagator is evaluated in a form linearized in the bound-state momentum variables [3]. Further, an approximate evaluation of the amplitude is considered which relies, in part, on the large size of the momentum transfer in comparison with the magnitude of the internuclear separation. This approximate version of the amplitude effectively separates the double-scattering aspect of the capture event from the diffraction aspect, thereby serving as a basis for comparison for the full B2 amplitude—the modification of the mechanism from the atomic case can be studied. Additionally, direct comparison with the atomic cross section is made.

At the high incident velocities considered in the present study, viz., 10 and 20 a.u. (2.5 and 10 MeV), the molecule does not have time to vibrate or rotate appreciably, owing to the short collision times involved [9]. Thus, the use of the fixed-nuclei approximation allows the capture amplitude to be taken as depending parametrically on the internuclear coordinate $\mathbf{R}$. Presently, no experimental data exist for capture from oriented hydrogen molecules, but the measurement of such cross sections, or of those for random orientations, is under development by two groups [10,11]. Previously, the Thomas mechanism has been studied experimentally in proton-hydrogen and proton-helium collisions [12]. To compare with cross sections obtained from a beam of protons incident on a gas of randomly oriented hydrogen molecules, an average can be made of all the fixed $\mathbf{R}$ cross sections. In its simplest form, this average can be taken by weighting equally the cross sections calculated at the experimental (equilibrium) value of the internuclear distance R_e for a discrete set of selected orientations.

The plan of the paper is the following. The second-order Born formalism is introduced and the amplitude reduced in Sec. II. Section III A presents calculated results for various molecular orientations. Section III B presents results averaged over all molecular orientations and compares them with the atomic case. Concluding remarks are made in Sec. IV. Atomic units are used.

*Permanent address.
†Present address: Department of Mathematics, Harvard University, Cambridge, MA 02138.
‡Present address: Department of Electrical Engineering and Computer Science, University of Michigan, Ann Arbor, MI 48109.

A plane-wave state $\phi_{\mathbf{k}}$ of momentum $\mathbf{k}$ and coordinate vector $\mathbf{r}$ is normalized as $\phi_{\mathbf{k}}(\mathbf{r}) = e^{i\mathbf{k}\cdot\mathbf{r}}$.

II. SECOND-ORDER BORN APPROXIMATION

The capture of an electron from a hydrogen molecule by a fast proton is considered assuming an effective one-electron model. At high velocities, the collision occurs so quickly that the molecule does not have time to rotate or vibrate appreciably [9]. Consequently, the fixed-nuclei approximation is assumed in the treatment of the collision in which the transition amplitude's dependence on the internuclear coordinate vector $\mathbf{R}$ connecting the two nuclei is taken as constant during the collision. The experimental value of the internuclear separation R_e is used. The exact transition amplitude for electron capture (in post form) is [13]

$$A(\mathbf{R}) = \langle \Phi_f | V_f | \Psi_i^+ \rangle, \tag{1}$$

where the dependence on the molecular orientation through the internuclear coordinate vector $\mathbf{R}$ is noted. The contribution of the internuclear potential (for the atomic case) to the second-order Born approximation has been shown to be negligible at forward scattering angles [6], if terms of the order of the electron mass over the heavy-particle masses are neglected. This analysis is carried over to the present case. Thus, the initial and final perturbations reduce to the single interactions

$$V_i = V_{Pe}(\mathbf{r}_P), \qquad V_f = V_{Te}(\mathbf{R}, \mathbf{r}_T), \tag{2}$$

where $\mathbf{r}_P$ and $\mathbf{r}_T$ denote the electron's position relative to the projectile-ion and target-ion centers of mass, respectively.

In the second-order Born approximation, the outgoing-wave initial scattering state is written as

$$|\Psi_i^+(\mathbf{R})\rangle \approx |\Psi_{B2}^+(\mathbf{R})\rangle \equiv [1 + G_0^+(E) V_{Pe}] |\Phi_i(\mathbf{R})\rangle, \tag{3}$$

where Eq. (2) has been used and the free Green operator is given by

$$G_0^+(E) = \left(E + \tfrac{1}{2\nu_i} \nabla_{\mathbf{R}_T}^2 + \tfrac{1}{2\mu} \nabla_{\mathbf{r}_T}^2 + i\eta \right)^{-1} \tag{4}$$

with $\mu = mM_T/(m + M_T) \approx m$ and $\eta \to 0+$. The total collision energy is $E = \frac{1}{2\nu_i} K_i^2 + \varepsilon_i = \frac{1}{2\nu_f} K_f^2 + \varepsilon_f$, where the three-body reduced masses are $\nu_i = M_P(m + M_T)/(m + M_P + M_T) \approx M_P M_T/(M_P + M_T)$ and $\nu_f = M_T(m + M_P)/(m + M_P + M_T) \approx M_P M_T/(M_P + M_T)$ with m, M_P, and M_T the electron, and projectile-ion and target-ion masses, respectively. The initial and final asymptotic scattering states Φ_i and Φ_f in Eqs. (1) and (3) are given in coordinate representation by

$$\begin{aligned} \Phi_i(\mathbf{R}, \mathbf{r}_T, \mathbf{R}_T) &= \phi_{\mathbf{K}_i}(\mathbf{R}_T) \phi_i(\mathbf{R}, \mathbf{r}_T), \\ \Phi_f(\mathbf{r}_P, \mathbf{R}_P) &= \phi_{\mathbf{K}_f}(\mathbf{R}_P) \phi_f(\mathbf{r}_P). \end{aligned} \tag{5}$$

In Eq. (5), the projectile's position relative to the target center of mass is denoted by $\mathbf{R}_P$, the target ion's position relative to the electron–projectile-ion center of mass is denoted by $\mathbf{R}_T$, and the initial and final heavy-particle wave vectors are $\mathbf{K}_i$ and $\mathbf{K}_f$. The initial molecular and final atomic bound-state wave functions are $\phi_i(\mathbf{R})$ and ϕ_f, respectively, and the corresponding energies are ε_i and ε_f.

Define the Fourier transform of a function $f(\mathbf{r})$ as

$$\tilde{f}(\mathbf{k}) = (2\pi)^{-3/2} \int d\mathbf{r}\, e^{-i\mathbf{k}\cdot\mathbf{r}} f(\mathbf{r}). \tag{6}$$

If the influence of the second electron is incorporated in the treatment, the electron–target-ion potential [Eq. (2)] becomes the sum of the two electron-nucleus potentials and the screened potential derived from the static charge distribution of the other electron

$$\begin{aligned} V_{Te}(\mathbf{R}, \mathbf{r}_T) = &-Z_T \left(|\mathbf{r}_T + \mathbf{R}/2|^{-1} + |\mathbf{r}_T - \mathbf{R}/2|^{-1} \right) \\ &+ \int d\mathbf{r}\, |\phi_i(\mathbf{R}, \mathbf{r})|^2 \, |\mathbf{r} - \mathbf{r}_T|^{-1}. \end{aligned} \tag{7}$$

The electron-projectile interaction is $V_{Pe}(\mathbf{r}_P) = -Z_P/r_P$. The Fourier transform of the electron–target-ion potential Eq. (7) can be evaluated to give

$$\begin{aligned} \tilde{V}_{Te}(\mathbf{R}, \mathbf{k}) = [&-2Z_T(2/\pi)^{1/2} \cos(\tfrac{1}{2}\mathbf{k}\cdot\mathbf{R}) \\ &+ 4\pi\tilde{\rho}(\mathbf{R}, \mathbf{k})]/k^2, \end{aligned} \tag{8}$$

where $\tilde{\rho}(\mathbf{R},\mathbf{k})$ denotes the Fourier transform of the single-occupation electronic charge density. Because of the cylindrical symmetry of the distribution, the ϕ_r integration in the transform of ρ can be done to give the real equation

$$\begin{aligned} \tilde{\rho}(\mathbf{R}, \mathbf{k}) = &(2\pi)^{-1/2} \int_0^\infty dr\, r^2 \\ &\times \int_0^\pi d\theta_r \, \sin\theta_r \, |\phi_i(\mathbf{R}, r, \theta_r)|^2 \\ &\times \cos(kr\cos\theta_k \cos\theta_r) \\ &\times J_0(kr \sin\theta_k \sin\theta_r). \end{aligned} \tag{9}$$

This expression for $\tilde{\rho}$ is evaluated using a double numerical integration [14]. Having now established the quantities in the formalism which depend on $\mathbf{R}$, explicit note of this dependence is suppressed in the further development below. As another check beyond the numerical convergence of the results of the program used for Eq. (9) it was verified that the small k limit gives the value $(2\pi)^{-3/2}$, representing the normalization of the wave function.

Using Eq. (6) for the bound-state wave functions and integrating the heavy-particle motion, the second-order Born amplitude can be put into the form

$$A_{B2} = A_{B1} + A_2, \tag{10}$$

where the first-order Born amplitude is

$$A_{B1} = -4\pi^3 (J^2 - 2\varepsilon_i) [\tilde{\phi}_f(\mathbf{K})]^* \, \tilde{\phi}_i(-\mathbf{J}) \tag{11}$$

and the second-order amplitude is

$$\begin{aligned} A_2 = &\int d\mathbf{k}_f d\mathbf{k}_i \, [\tilde{\phi}_f(\mathbf{k}_f)]^* \, \tilde{V}_{Te}(\mathbf{k}_i + \mathbf{J}) \, \tilde{G}_0^+(E) \\ &\times \tilde{V}_{Pe}(\mathbf{k}_f - \mathbf{K}) \, \tilde{\phi}_i(\mathbf{k}_i) \end{aligned} \tag{12}$$

with

$$\tilde{G}_0^+(E) = \left[\varepsilon - \tfrac{1}{2}(\mathbf{k}_i + \mathbf{k}_f + \mathbf{J})^2 + i\eta\right]^{-1} \tag{13}$$

and $\varepsilon = \frac{1}{2}v^2 - \mathbf{v}\cdot\mathbf{k}_i + \varepsilon_i$. The momentum transfers experienced by the target and projectile ions, respectively, are denoted here by $\mathbf{J} = \alpha\mathbf{K}_i - \mathbf{K}_f$ and $\mathbf{K} = \beta\mathbf{K}_f - \mathbf{K}_i$. Each is the sum of components parallel and perpendicular to the projectile velocity $\mathbf{v}$: $K_\parallel = -\frac{1}{2}v + (\varepsilon_i - \varepsilon_f)/v$, $J_\parallel = -\frac{1}{2}v + (\varepsilon_f - \varepsilon_i)/v$; $K_\perp$ for $\mathbf{K}$, $-K_\perp$ for $\mathbf{J}$. For the calculations reported below, $\mathbf{K}_\perp$ is taken along the positive x axis, $\Phi_\mathbf{K} = 0°$; $\mathbf{J}_\perp$ is then along the negative x axis. Momentum conservation for the process takes the form $\mathbf{K} + \mathbf{J} + \mathbf{v} = \mathbf{0}$ [15]. Figure 1, which is not to scale, shows the relative orientations and defines the angles of the molecular axis $\mathbf{R}$, the momentum transfers $\mathbf{K}$ and $\mathbf{J}$, and $\mathbf{v}$. The positive z direction in the laboratory frame is taken along $\mathbf{v}$.

It has been shown that the Thomas-peak enhancement derives from a singularity in Eq. (13), the momentum-space counterpart of the free Green function Eq. (4) [3]. Consequently, the Green function can be approximated by a form linear in the momentum variables:

$$\tilde{G}_0^+(E) \approx (\alpha + \mathbf{k}_i\cdot\mathbf{K} - \mathbf{k}_f\cdot\mathbf{J} + i\eta)^{-1}, \tag{14}$$

with $\alpha = \frac{1}{2}(v^2 - K^2 + 2\varepsilon_f)$ and $\eta \to 0+$. The singularity occurs at $\alpha = 0$. Additionally, the momentum dependencies of the potentials are neglected. If these approximations are made in Eq. (12), a quantity I can be defined by

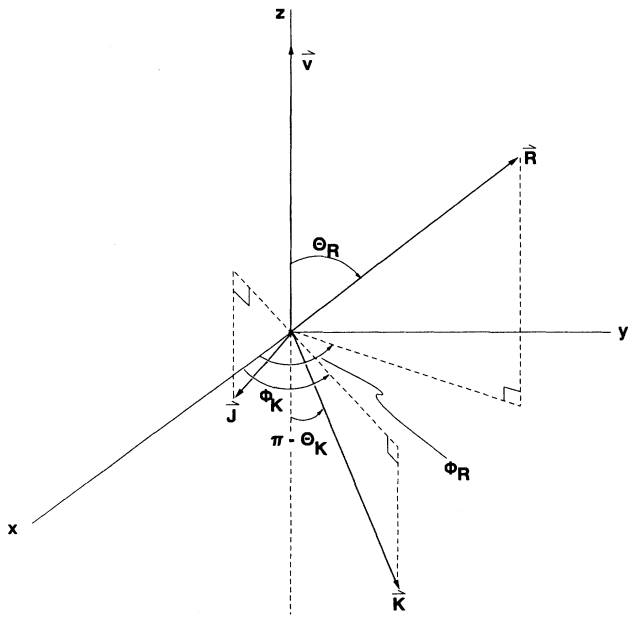

FIG. 1. Diagram showing the relative orientations and defining angles of the molecular axis (internuclear coordinate vector) $\mathbf{R}$, the momentum $\mathbf{K}$ transferred to the projectile, the momentum $\mathbf{J}$ transferred to the target core, and the projectile velocity $\mathbf{v}$, which is taken along the positive z direction in the laboratory frame (not to scale).

$$A_2 \approx \tilde{V}_{Te}(\mathbf{J})\, I\, \tilde{V}_{Pe}(-\mathbf{K}) \tag{15}$$

with

$$I \equiv \int d\mathbf{k}_f d\mathbf{k}_i\, [\tilde{\phi}_f(\mathbf{k}_f)]^*\, \tilde{G}_0^+(E)\, \tilde{\phi}_i(\mathbf{k}_i). \tag{16}$$

The angular integration over $\hat{\mathbf{k}}_f$ in Eq. (16) can be straightforwardly performed; the remaining radial integration over k_f can be done by completing the integration contour in the upper half-plane and obtaining the residue at $+iZ_P$, giving a quantity $D^{-1} = (\alpha + iZ_P J + \mathbf{K}\cdot\mathbf{k}_i)^{-1}$. Recall that the $1s$ hydrogenic wave function in momentum space is $\tilde{\phi}_{1s}(\mathbf{k}) = (2^3 Z_P^5)^{1/2}/\pi(k^2 + Z_P^2)^2$. The $\mathbf{k}_i$ integration cannot be done in simple closed form, except approximately as shown below. For the evaluation of the momentum integral, it is convenient to introduce the integral representation

$$D^{-1} = \int_0^\infty dx\, e^{ixD}.$$

Equation (16) takes the form

$$\begin{aligned} I &= -i\pi(2Z_P)^{3/2} \int d\mathbf{k}_i \int_0^\infty dx\, e^{ix(\alpha + iZ_P J + \mathbf{K}\cdot\mathbf{k}_i)} \tilde{\phi}_i(\mathbf{k}_i) \\ &= -i2^3\pi(\pi Z_P)^{3/2} \int_0^\infty dx\, e^{ix(\alpha + iZ_P J)} \phi_i(x\mathbf{K}), \end{aligned} \tag{17}$$

where the x and $\mathbf{k}_i$ integrations have been interchanged, which is valid since the integrand is asymptotically well defined. Equation (17) is evaluated numerically. Thus, the amplitude Eq. (10) consists in the use of Eq. (11) and Eq. (15) with Eqs. (8), (9), and (17). A computer program written in C was used to perform the calculations. The x integration was converged to six digits of accuracy. Furthermore, the limit of the amplitude as $R \to 0$ was checked for reproduction of the atomic cross section. See after Eq. (21) below.

The Hartree-Fock $^1\Sigma_g$ molecular wave function used is close to the converged HF limit. It is a product of three-function molecular orbitals [8]. The molecular orbital in coordinate representation, which is used in Eq. (17), is of the form

$$\phi_i(\mathbf{r}) = a_{1s}\phi_{1s}(\mathbf{r}) + a_{2s}\phi_{2s}(\mathbf{r}) + a_{2p_0}\phi_{2p_0}(\mathbf{r}), \tag{18}$$

where the σ_g symmetry orbitals are

$$\begin{aligned} \phi_{1s}(\mathbf{r}) &= \chi_{1s}(\mathbf{r} + \mathbf{R}/2) + \chi_{1s}(\mathbf{r} - \mathbf{R}/2), \\ \phi_{2s}(\mathbf{r}) &= \chi_{2s}(\mathbf{r} + \mathbf{R}/2) + \chi_{2s}(\mathbf{r} - \mathbf{R}/2), \\ \phi_{2p_0}(\mathbf{r}) &= \chi_{2p_0}(\mathbf{r} + \mathbf{R}/2) - \chi_{2p_0}(\mathbf{r} - \mathbf{R}/2). \end{aligned}$$

The (normalized) Slater orbitals are [16]

$$\begin{aligned} \chi_{1s}(\mathbf{r}) &= 2\zeta_1^{3/2} e^{-\zeta_1 r}\, Y_{00}, \\ \chi_{2s}(\mathbf{r}) &= 2(\zeta_2^5/3)^{1/2} r e^{-\zeta_2 r}\, Y_{00}, \\ \chi_{2p_0}(\mathbf{r}) &= 2(\zeta_3^5/3)^{1/2} r e^{-\zeta_3 r}\, Y_{10}(\theta_r, \phi_r), \end{aligned}$$

with $Y_{00} = (1/4\pi)^{1/2}$ and $Y_{10}(\theta_r, \phi_r) = (3/4\pi)^{1/2}\cos\theta_r$. Angles are defined relative to the internuclear axis $\hat{\mathbf{R}}$.

The Hartree-Fock approximation gives the coefficients in Eq. (18) as $a_{1s} = 0.432\,62$, $a_{2s} = 0.123\,81$, and $a_{2p_0} = 0.028\,27$. They are scaled so that the wave function is normalized. The orbital exponents are also optimized in the Hartree-Fock calculation to give $\zeta_1 = 1.378$, $\zeta_2 = 1.176$, and $\zeta_3 = 1.820$. The orbital energy found for the ground state is $\varepsilon_i = \varepsilon_{1\sigma_g} = -0.594\,43$ a.u. (16.175 eV), giving a total molecular energy of -1.1335 a.u. (30.295 eV), which is 96.5% of the experimental value.

The momentum-space representation of the wave function is

$$\tilde{\phi}_i(\mathbf{k}) = a_{1s}\tilde{\phi}_{1s}(\mathbf{k}) + a_{2s}\tilde{\phi}_{2s}(\mathbf{k}) + a_{2p_0}\tilde{\phi}_{2p_0}(\mathbf{k}), \quad (19)$$

where the σ_g symmetry orbitals are

$$\tilde{\phi}_{1s}(\mathbf{k}) = 2\cos(\mathbf{k}\cdot\mathbf{R}/2)\tilde{\chi}_{1s}(\mathbf{k}),$$
$$\tilde{\phi}_{2s}(\mathbf{k}) = 2\cos(\mathbf{k}\cdot\mathbf{R}/2)\tilde{\chi}_{2s}(\mathbf{k}),$$
$$\tilde{\phi}_{2p_0}(\mathbf{k}) = 2i\sin(\mathbf{k}\cdot\mathbf{R}/2)\tilde{\chi}_{2p_0}(\mathbf{k}).$$

The momentum-space Slater orbitals are

$$\tilde{\chi}_{1s}(\mathbf{k}) = (2^5\zeta_1^5/\pi)^{1/2}(k^2+\zeta_1^2)^{-2}\,Y_{00},$$
$$\tilde{\chi}_{2s}(\mathbf{k}) = (2^5\zeta_2^5/3\pi)^{1/2}(3\zeta_2^2-k^2)(k^2+\zeta_2^2)^{-3}\,Y_{00},$$
$$\tilde{\chi}_{2p_0}(\mathbf{k}) = -4i\zeta_3(2^5\zeta_3^5/3\pi)^{1/2}k(k^2+\zeta_3^2)^{-3}\,Y_{10}(\theta_k,\phi_k).$$

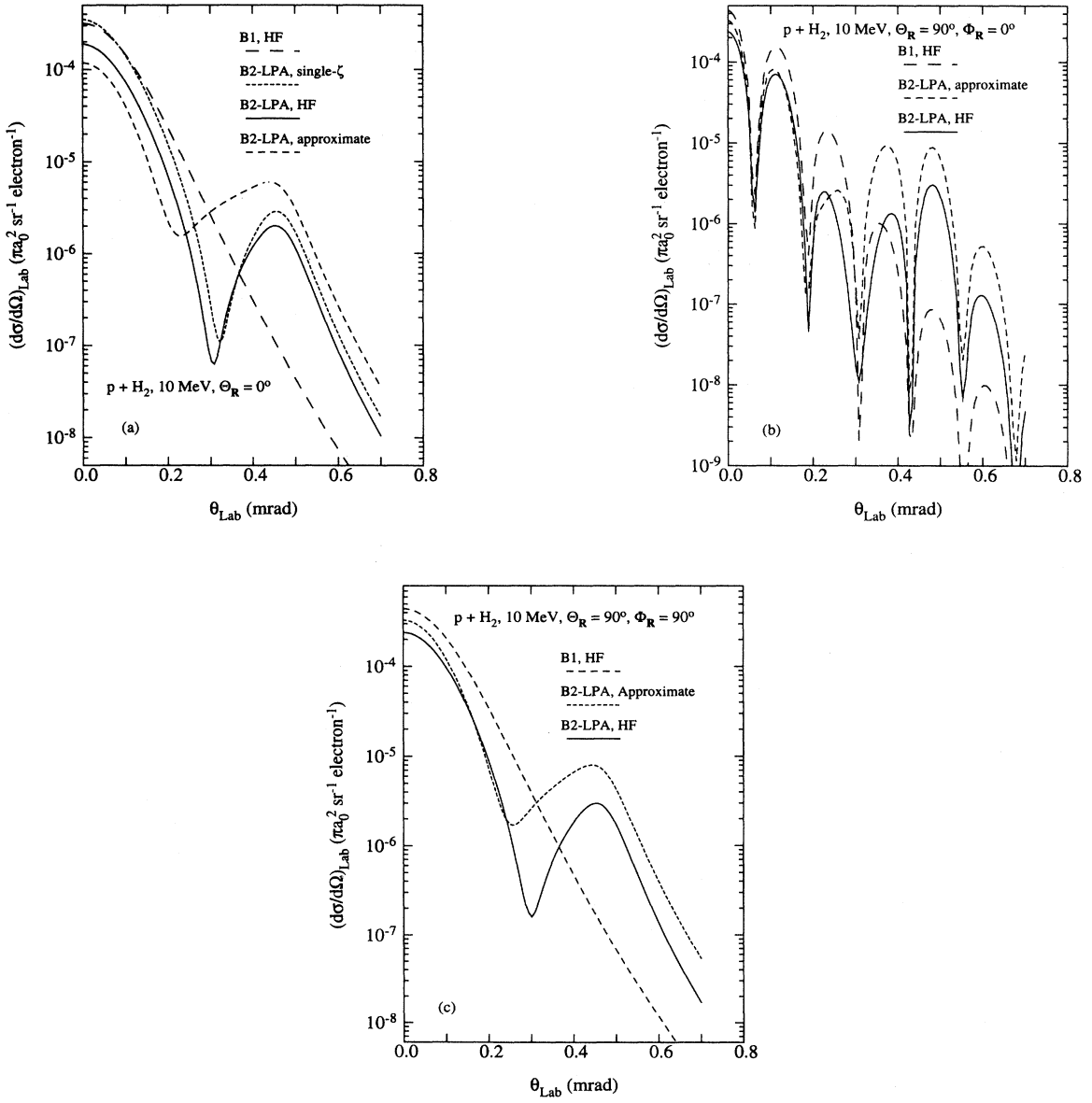

FIG. 2. Differential capture cross sections for protons incident at 10 MeV on hydrogen molecules at three orientations: (a) For $\Theta_{\mathbf{R}} = 0°$, $\Phi_{\mathbf{R}} = 0°$, the results are for the second-order Born amplitude in the linearized-propagator approximation (B2-LPA) using a Hartree-Fock (HF) or a single-ζ molecular wave function, for the first-order Born (B1) approximation with HF wave function, and for the approximate evaluation of the B2-LPA in Eq. (21); (b) for $\Theta_{\mathbf{R}} = 90°$, $\Phi_{\mathbf{R}} = 0°$, same as (a) with the single-ζ curve omitted; (c) for $\Theta_{\mathbf{R}} = 90°$, $\Phi_{\mathbf{R}} = 90°$, same as (a) with the single-ζ curve omitted.

Equation (19) is used in the first-order Born amplitude Eq. (11).

The fundamental modification of the capture amplitude for a molecular H_2 target in comparison with that for an atomic H target can be obtained by using a molecular wave function consisting of the product molecular orbitals which are the sum of $1s$ atomic orbitals $e^{-\zeta|\mathbf{r}\pm\mathbf{R}/2|}$. This construction has been carried out long ago, leading to a variationally determined charge of $\zeta = 1.1930$ [17]. The normalization factor for this function is $N(R) = (2 + 2S)^{-1/2}$, where $S(R) = e^{-\zeta R}[1 + \zeta R + (\zeta R)^2/3]$. While this orbital does not give a good dissociation energy for the molecule, it does give a good value for the equilibrium separation of the nuclei of $R = 1.38$ a.u. (versus the experimental value 1.402).

Using this single-ζ molecular orbital, the integral in Eq. (17) becomes

$$I = -i2^3\pi^2(\zeta Z_P)^{3/2}N\int_0^\infty dx\, e^{ix(\alpha+iZ_PJ)} \times\left(e^{-\zeta|x\mathbf{K}+\mathbf{R}/2|}+e^{-\zeta|x\mathbf{K}-\mathbf{R}/2|}\right). \quad (20)$$

This integral can be evaluated analytically if it is assumed that $xK \gg R/2$, so that $|x\mathbf{K}\pm\mathbf{R}/2| \approx xK \pm \mathbf{R}/2$. Since $2K \sim v$ and $R \sim 1$, one needs at least $x \sim v^{-1}$ as the region giving the main contribution to the integral I. This is not achieved to good approximation, even for higher velocities; nevertheless, an approximate amplitude is useful for understanding the modification of the process. On evaluating Eq. (20), one finds for Eq. (15) the simple approximate expression

$$A_2 \approx 4\pi^2(2N)(\zeta Z_P)^{3/2}\,\tilde{V}_{Te}(\mathbf{J})\tilde{V}_{Pe}(-\mathbf{K}) \times\cosh[\tfrac{1}{2}(\zeta\hat{\mathbf{K}})\cdot\mathbf{R}]\,[\alpha + i(Z_PJ + \zeta K)]^{-1}. \quad (21)$$

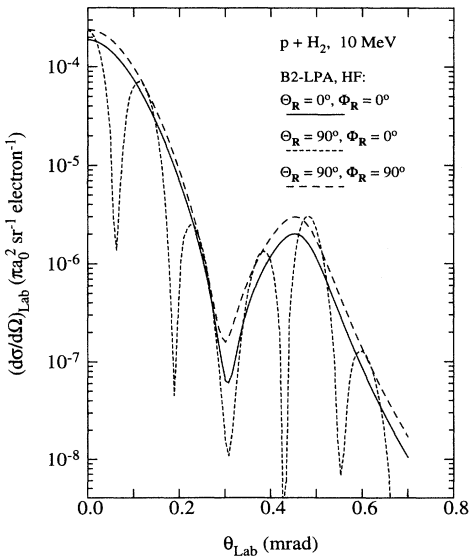

FIG. 3. Comparative differential capture cross sections calculated using the B2-LPA for protons incident at 10 MeV on hydrogen molecules at three orthogonal orientations: $\Theta_\mathbf{R} = 0°$, $\Phi_\mathbf{R} = 0°$; $\Theta_\mathbf{R} = 90°$, $\Phi_\mathbf{R} = 0°$; and $\Theta_\mathbf{R} = 90°$, $\Phi_\mathbf{R} = 90°$.

In the united-atom limit where $R \to 0$, one has $2N \to 1$, $\cosh[\frac{1}{2}(\zeta\hat{\mathbf{K}})\cdot\mathbf{R}] \to 1$, and in the potential $\tilde{V}_{Te}$, $\cos(\frac{1}{2}\mathbf{J}\cdot\mathbf{R}) \to 1$. Thus, the second-order amplitude A_2 goes over explicitly to the atomic amplitude. The Thomas peak occurs at $\alpha = 0$. A similar limit exists for A_{B1}. For the molecular case, although the peak location is not altered, the magnitude and shape of the peak are affected by the interference arising from the presence of the $\cosh[\frac{1}{2}(\zeta\hat{\mathbf{K}})\cdot\mathbf{R}]$ and $\cos(\frac{1}{2}\mathbf{J}\cdot\mathbf{R})$ factors in A_2. (Also, $\tilde{\rho}$ can play a small role.)

The approximation used in evaluating Eq. (20) can be employed, with parametric differentiation involved also, to obtain an amplitude generalizing Eq. (21) when the Hartree-Fock wave function is used in place of the single-ζ function. Relative to what is shown in Figs. 2 and 6 below using Eq. (21), the approximate HF cross sections differ only slightly. Thus, since the generalized expression is rather more complicated and not as intuitive, it is not employed in the calculations reported below and not discussed further.

The differential cross section, for a given internuclear separation R and molecular orientation $\hat{\mathbf{R}}$, is given by

$$\left(\frac{d\sigma(\mathbf{R})}{d\Omega}\right)_{\text{lab}} = \frac{(1+\tau)^{1/2}}{\pi}\left(\frac{\mu}{2\pi}\right)^2|A_{\text{B2}}(\mathbf{R},K_\perp)|^2, \quad (22)$$

where $K_\perp = 2\mu v\sin(\theta_{\text{c.m.}}/2)$. The center-of-mass scattering angle is related to the laboratory scattering angle as $\theta_{\text{c.m.}} = (1+\tau)\theta_{\text{lab}}$ with $\tau = m_p/(2m_p) = \frac{1}{2}$ for protons incident on hydrogen molecules; the reduced mass is $\mu = (2m_p)m_p/(2m_p + m_p) \approx \frac{2}{3}m_p$ [11].

III. RESULTS AND DISCUSSION

In this section differential cross sections for electron capture from hydrogen molecules by protons are presented. The experimental equilibrium internuclear separation $R = 1.402$ au is used in the calculations. The cross sections are calculated from 0 mrad to 0.7 mrad in 0.01 mrad intervals (71 total points). Section III A presents a discussion of the cross sections for different $\hat{\mathbf{R}}$. Because of the symmetry of the capture process for an inversion of $\mathbf{R}$, i.e., for $\Theta_\mathbf{R} \to 180° - \Theta_\mathbf{R}$ and $\Phi_\mathbf{R} \to 180° + \Phi_\mathbf{R}$, there is no need to present cross sections for $180° < \Phi_\mathbf{R} \le 360°$. The computer program has been checked at a number of angle pairs, e.g., $\Theta_\mathbf{R} = 0°$ and $\Theta_\mathbf{R} = 180°$; $\Theta_\mathbf{R} = 30°$, $\Phi_\mathbf{R} = 0°$ and $\Theta_\mathbf{R} = 150°$, $\Phi_\mathbf{R} = 180°$; and $\Theta_\mathbf{R} = 30°$, $\Phi_\mathbf{R} = 90°$ and $\Theta_\mathbf{R} = 150°$, $\Phi_\mathbf{R} = 270°$, to ensure that it gives, after full calculations, identical cross sections. In Sec. III B, differential cross sections averaged over all orientations are presented.

A. Capture from oriented molecules

Differential electron capture cross sections are shown in Fig. 2 for protons incident at 10 MeV on hydrogen molecules at three different orientations. This high energy corresponds to a velocity of about 20 a.u. First,

in Fig. 2(a), for the molecule aligned along the projectile velocity, i.e., for the angles $\Theta_{\mathbf{R}} = 0°$, $\Phi_{\mathbf{R}} = 0°$, the calculated results are for the second-order Born amplitude in the linearized-propagator approximation (B2-LPA) with HF and single-ζ molecular wave functions, the first-order Born (B1) approximation with HF wave function, and the approximate evaluation of the B2-LPA given in Eq. (21). The pronounced peak of the Thomas mechanism is readily apparent at 0.47 mrad. It is seen that a single-ζ molecular orbital gives a substantially different cross section. The differences between the HF and single-ζ results are considerably larger than the similar differences found in proton-helium collisions. This can be attributed to the rather poor representation of the molecule provided by the single-ζ function [17]. The relative magnitudes and positions of the B1 and B2 cross sections are comparable to what are seen in proton-hydrogen atom collisions.

A significant result of the present work, and one that is somewhat surprising in view of the discussion following Eq. (20), is shown in Fig. 2(a). The approximate amplitude separating double scattering and diffraction gives a poor representation of molecular capture. As was noted in the discussion after Eq. (21), this failure cannot be attributed to the poor modeling of the molecule by the single-ζ function. The cross section obtained using the HF wave function Eq. (18) and similar approximate evaluation leading from Eq. (20) to Eq. (21) differs very little from the plotted curve. Thus, fundamentally, the separa-

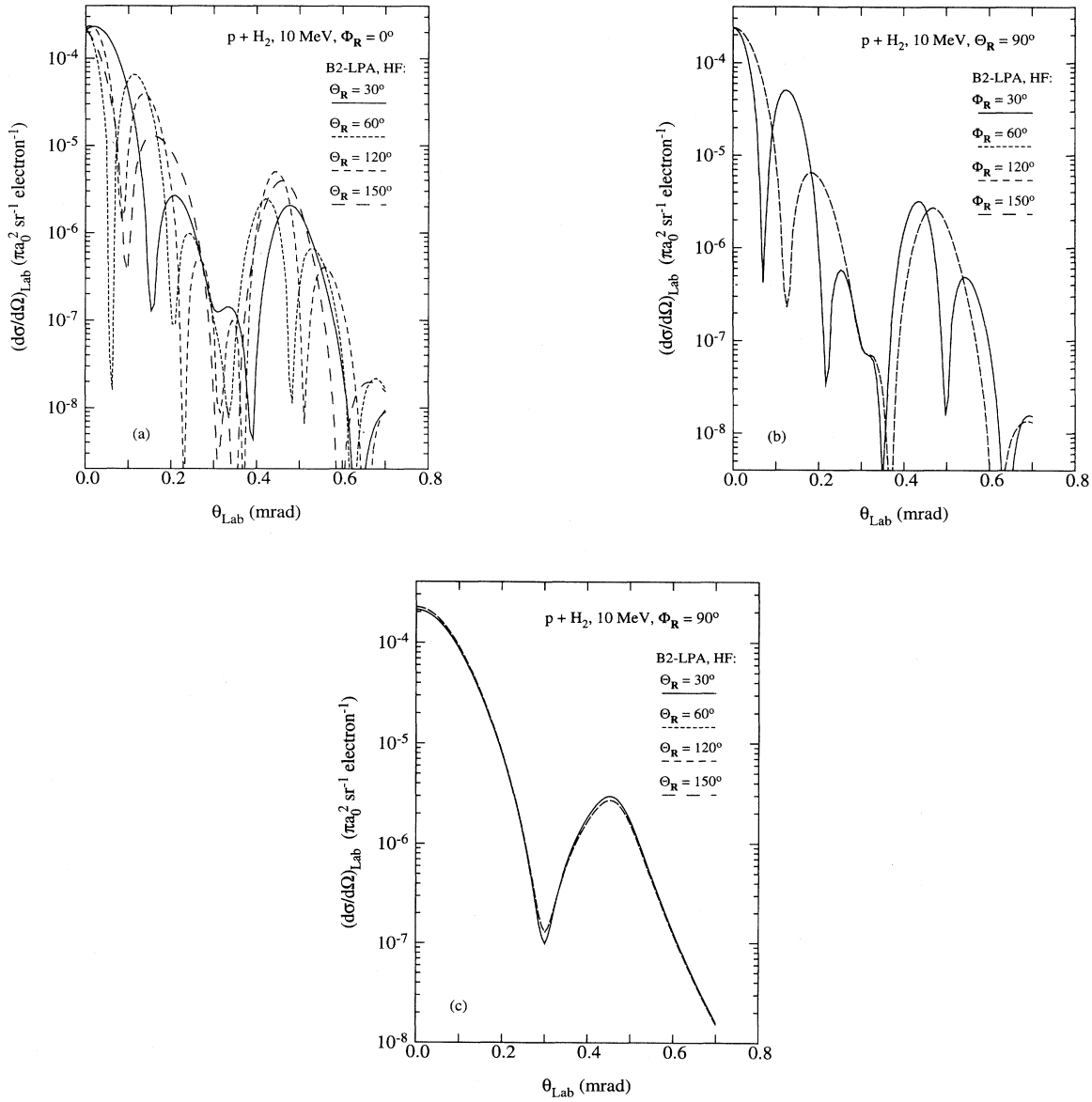

FIG. 4. Comparative differential capture cross sections calculated using the B2-LPA for protons incident at 10 MeV on hydrogen molecules at three sets of orientations: (a) $\Theta_{\mathbf{R}} = 0°$, $\Phi_{\mathbf{R}} = 30°$, 60°, 120°, and 150°; (b) $\Theta_{\mathbf{R}} = 90°$, $\Phi_{\mathbf{R}} = 30°$, 60°, 120°, and 150°; and (c) $\Theta_{\mathbf{R}} = 30°$, 60°, 120°, and 150°, $\Phi_{\mathbf{R}} = 90°$.

tion of the double-scattering aspect of the capture event from the diffraction aspect is not a good approximation—the two aspects do not evolve independently.

In Fig 2(b), for $\Theta_{\mathbf{R}} = 90°$, $\Phi_{\mathbf{R}} = 0°$, representing capture from a molecule oriented perpendicularly to the beam direction in the plane containing the transverse momentum transfer vector (the **v**-**K** plane), results using the same amplitudes as in Fig. 2(a) are shown, except for the single-ζ result. The single-ζ results are not shown because of the poor modeling of the molecule by the single-ζ orbital relative to the accurate molecular-orbital results. Diffraction effects are pronounced in this figure. (The sharp localized minima in the cross sections correspond to zeros in the amplitudes; they do not appear exactly as such because the cross sections are calculated at a discrete set of projectile scattering angles and the plot ordinates are on a logarithmic scale.) It is seen that the B2 cross section still dominates the B1 cross section in the Thomas peak region.

In Fig. 2(c), for $\Theta_{\mathbf{R}} = 90°$, $\Phi_{\mathbf{R}} = 90°$, for the molecule perpendicular to both the beam direction and the transverse momentum transfer (recalling that $\mathbf{K}_\perp$ is along the positive x axis), results are shown for the same amplitudes, except for the omitted single-ζ curve. Here, it is

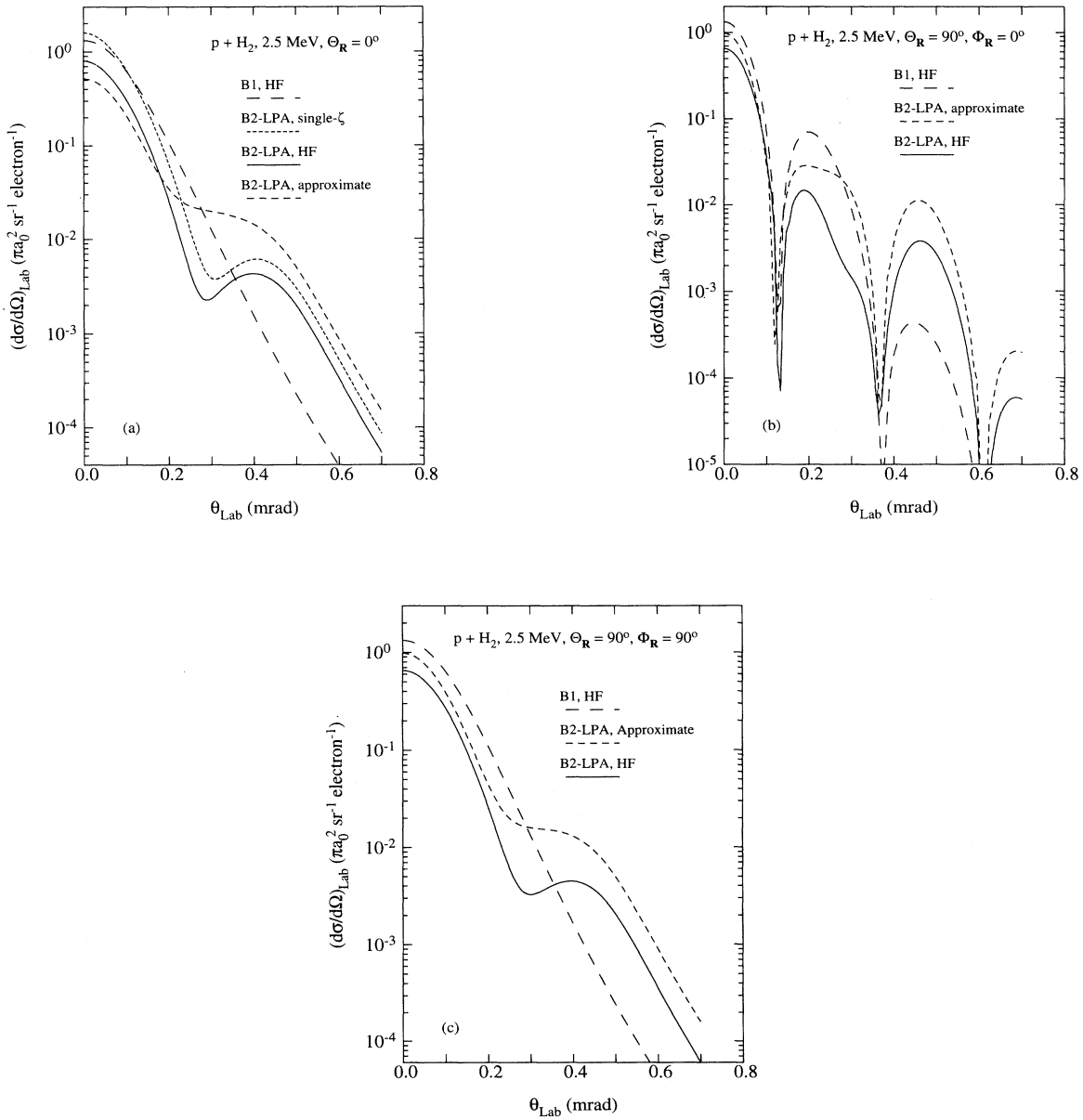

FIG. 5. Differential capture cross sections for protons incident at 2.5 MeV on hydrogen molecules at three orientations: (a) For $\Theta_{\mathbf{R}} = 0°$, $\Phi_{\mathbf{R}} = 0°$, the results are B2-LPA with HF or single-ζ molecular wave function, the B1 approximation with HF wave function, and an approximate evaluation of the B2-LPA; (b) for $\Theta_{\mathbf{R}} = 90°$, $\Phi_{\mathbf{R}} = 0°$, same as (a) with the single-ζ curve omitted; (c) for $\Theta_{\mathbf{R}} = 90°$, $\Phi_{\mathbf{R}} = 90°$, same as (a) with the single-ζ curve omitted.

seen that the diffraction effects do not arise because the variable part of the momentum transfer is perpendicular to the plane of the two molecular nuclei. The approximate amplitude gives a somewhat better representation of the capture at this orientation.

In Fig. 3, a direct comparison is shown for protons incident at 10 MeV on hydrogen molecules of the HF B2-LPA differential capture cross sections for the three orthogonal orientations: $\Theta_{\mathbf{R}} = 0°$, $\Phi_{\mathbf{R}} = 0°$; $\Theta_{\mathbf{R}} = 90°$, $\Phi_{\mathbf{R}} = 0°$; and $\Theta_{\mathbf{R}} = 90°$, $\Phi_{\mathbf{R}} = 90°$. Around 0 mrad, the results for the fully perpendicular orientation are about 30% higher than for the forward molecular alignment and 50% higher at the Thomas peak. These differences are seen also in cross section for the approximate evaluation. A consideration of Eqs. (21) and (8) shows the likely cause of the increase to be the cosine term in the potential $\tilde{V}_{Te}$.

To give a broader view of the variation of the cross section versus molecular orientation, Fig. 4 presents differential capture cross sections calculated using the B2-LPA for protons incident at 10 MeV for three sets of orientations: (a) $\Theta_{\mathbf{R}} = 0°$, $\Phi_{\mathbf{R}} = 30°$, 60°, 120°, and 150°; (b) $\Theta_{\mathbf{R}} = 90°$, $\Phi_{\mathbf{R}} = 30°$, 60°, 120° , and 150°; and (c) $\Theta_{\mathbf{R}} = 30°$, 60° , 120°, and 150°, $\Phi_{\mathbf{R}} = 90°$. These figures show how the diffraction varies as the molecular orientation varies, a behavior resulting primarily from the magnitude of the projection of $\mathbf{K}$ on $\mathbf{R}$, which appears in the cosine term in $\tilde{V}_{Te}$. It is seen in Fig. 4(a), in particular, that the Thomas peak may be little affected, as for $\Theta_{\mathbf{R}} = 0°$, $\Phi_{\mathbf{R}} = 30°$, or it may contain a "hole," as for $\Theta_{\mathbf{R}} = 0°$, $\Phi_{\mathbf{R}} = 60°$. In addition to the $\mathbf{R}$ inversion symmetry mentioned previously, two other symmetries are apparent in Figs. 4(b) and 4(c). In the first, for $\Theta_{\mathbf{R}} = 90°$, the symmetry with respect to $\mathbf{K}_\perp$ is shown. The cross sections for $\Phi_{\mathbf{R}} = 30°$ and $\Phi_{\mathbf{R}} = 150°$ and for $\Phi_{\mathbf{R}} = 60°$ and $\Phi_{\mathbf{R}} = 120°$ are identical. In the second, for $\Phi_{\mathbf{R}} = 90°$, the symmetry as the molecule is rotated in the plane perpendicular to $\mathbf{K}_\perp$ is shown. The cross sections for $\Phi_{\mathbf{R}} = 30°$, 60°, 120°, and 150° are very similar, with those for the molecule aligned more along the incident direction being slightly larger in the Thomas peak region. Concerning Figs. 4(b) and 4(c), one should note that the x integral of Eq. (17) also plays a role in determining the $\mathbf{K}$ dependence of the amplitude.

Differential electron capture cross sections are now presented in Fig. 5 for protons incident at 2.5 MeV on hydrogen molecules at three different orientations. This intermediate energy corresponds to a velocity of about 10 a.u. For perspective, it may be noted that for protons on hydrogen atoms at this energy the Thomas peak is reduced to just a shoulder (see below). For the molecule aligned along the projectile velocity, i.e., for the angles $\Theta_{\mathbf{R}} = 0°$, $\Phi_{\mathbf{R}} = 0°$, Fig. 5(a) shows calculated results obtained using the B2-LPA with the HF and single-ζ molecular wave functions, the B1 approximation with the HF wave function, and the approximate B2-LPA. Surprisingly, the Thomas peak is still apparent at this energy. The single-ζ molecular orbital gives a substantially different cross section, slightly more so than at 10 MeV. Again, the poor representation of the molecule provided by the single-ζ function is the reason [17]. The relative magnitudes and positions of the B1 and B2 cross sections are comparable to what is seen in proton-hydrogen atom collisions. The poor representation of capture given by the approximate amplitude, which was seen in Fig. 2, is even poorer here, giving only a shoulder instead of a Thomas peak (as in the atomic case). The separation of the double-scattering aspect of the capture event from the diffraction aspect is an even worse approximation at the lower energy.

In Fig. 5(b), for $\Theta_{\mathbf{R}} = 90°$, $\Phi_{\mathbf{R}} = 0°$, for the molecule perpendicular to the beam direction in the plane containing $\mathbf{K}$, results using the same amplitudes as in Fig. 5(a) are shown, except for omitted single-ζ result. The diffraction effects are pronounced in this figure also, but occur half as frequently since the momentum transfer is roughly half of its value at the high energy. It is seen, however, that the B2 cross section still dominates the B1 cross section in the Thomas peak region. In Fig. 5(c), for $\Theta_{\mathbf{R}} = 90°$, $\Phi_{\mathbf{R}} = 90°$, for the molecule perpendicular to both the beam direction and $\mathbf{K}_\perp$, results are shown for the same amplitudes, except for the omitted single-ζ curve. Here, the diffraction effects do not arise because the variable part of the momentum is perpendicular to the plane of the two molecular nuclei. The approximate amplitude does somewhat better at this orientation.

In Fig. 6, a direct comparison is shown for protons incident at 2.5 MeV and the molecule of the HF B2-LPA cross sections for the three orthogonal orientations: $\Theta_{\mathbf{R}} = 0°$, $\Phi_{\mathbf{R}} = 0°$; $\Theta_{\mathbf{R}} = 90°$, $\Phi_{\mathbf{R}} = 0°$; and $\Theta_{\mathbf{R}} = 90°$, $\Phi_{\mathbf{R}} = 90°$. For the HF B2-LPA approximation, the fully perpendicular results are about 20% higher than those for the forward molecular alignment at 0 mrad and marginally higher at the Thomas peak. These differences are seen also in the cross sections for the approximate amplitude.

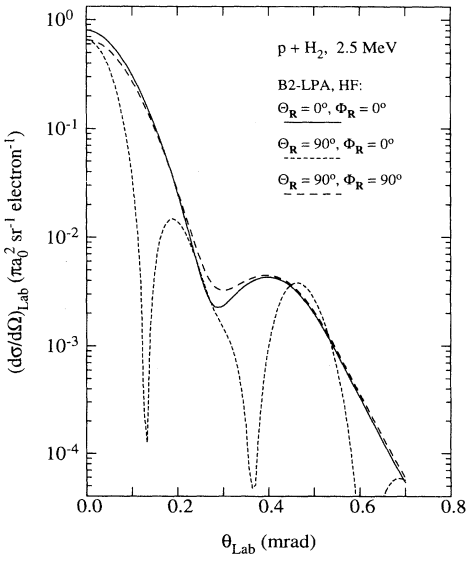

FIG. 6. Comparative differential capture cross sections calculated using the B2-LPA for protons incident at 2.5 MeV on hydrogen molecules at three orthogonal orientations: $\Theta_{\mathbf{R}} = 0°$, $\Phi_{\mathbf{R}} = 0°$; $\Theta_{\mathbf{R}} = 90°$, $\Phi_{\mathbf{R}} = 0°$; and $\Theta_{\mathbf{R}} = 90°$, $\Phi_{\mathbf{R}} = 90°$.

Figure 7 presents differential capture cross sections calculated using the B2-LPA for protons incident at 2.5 MeV for three sets of orientations: (a) $\Theta_{\mathbf{R}} = 0°$, $\Phi_{\mathbf{R}} = 30°$, 60°, 120°, and 150°; (b) $\Theta_{\mathbf{R}} = 90°$, $\Phi_{\mathbf{R}} = 30°$, 60°, 120°, and 150°; and (c) $\Theta_{\mathbf{R}} = 30°$, 60°, 120°, and 150°, $\Phi_{\mathbf{R}} = 90°$. These figures show again how the diffraction varies as the molecular orientation varies, but now with less oscillation because of the smaller velocity. Figure 7(a) shows a forward-scattering angle dip for $\Theta_{\mathbf{R}} = 60°$, $\Theta_{\mathbf{R}} = 120°$, but the Thomas peak is largely unaffected, or it may contain a "hole," as for $\Theta_{\mathbf{R}} = 90°$, $\Phi_{\mathbf{R}} = 30°$. In addition to the $\mathbf{R}$ inversion, the two other symmetries are apparent in Figs. 7(b) and 7(c) also. In the first, for $\Theta_{\mathbf{R}} = 90°$, the symmetry with respect to $\mathbf{K}_\perp$ is shown. The cross sections for $\Phi_{\mathbf{R}} = 30°$ and $\Phi_{\mathbf{R}} = 150°$ and for $\Phi_{\mathbf{R}} = 60°$ and $\Phi_{\mathbf{R}} = 120°$ are identical. In the second, for $\Phi_{\mathbf{R}} = 90°$, the symmetry as the molecule is rotated in the plane perpendicular to $\mathbf{K}_\perp$ is shown. The cross sections shown in Fig. 7(c) for $\Phi_{\mathbf{R}} = 30°$ and 150° are very different from those for $\Phi_{\mathbf{R}} = 60°$ and 120°. Those for the molecule aligned more along the incident direction are some 50 times larger.

B. Capture from randomly oriented molecules

For capture from a gas of randomly oriented molecules, the calculated differential cross section in the adiabatic-

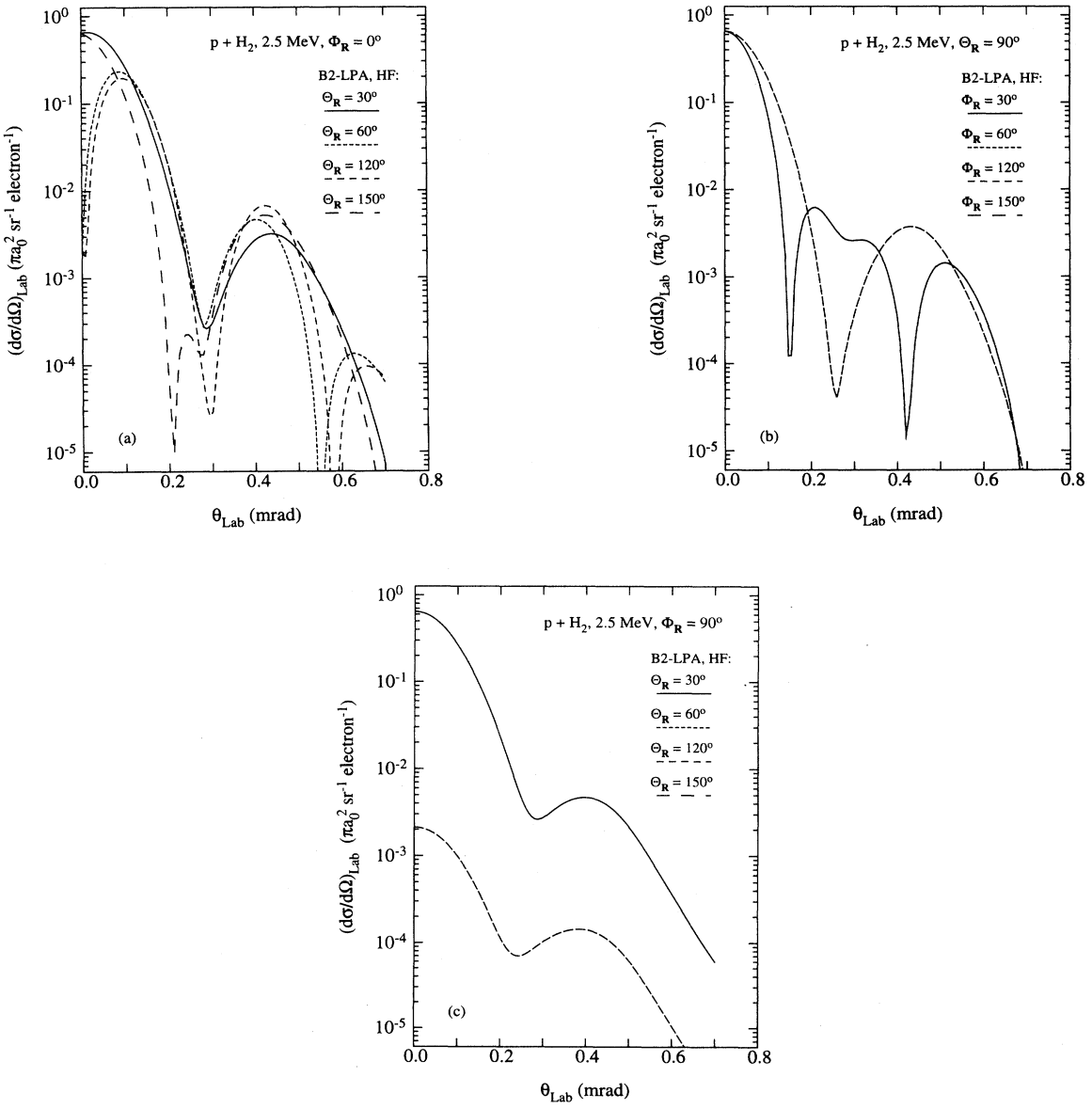

FIG. 7. Comparative differential capture cross sections calculated using the B2-LPA for protons incident at 2.5 MeV on hydrogen molecules at three sets of orientations: (a) $\Theta_{\mathbf{R}} = 0°$, $\Phi_{\mathbf{R}} = 30°$, 60°, 120°, and 150°; (b) $\Theta_{\mathbf{R}} = 90°$, $\Phi_{\mathbf{R}} = 30°$, 60°, 120°, and 150°; and (c) $\Theta_{\mathbf{R}} = 30°$, 60°, 120°, and 150°, $\Phi_{\mathbf{R}} = 90°$.

nuclei approximation should be averaged over all possible orientations, both $\Theta_{\mathbf{R}}$ and $\Phi_{\mathbf{R}}$. An equal weighting of all orientations is used:

$$\left\langle \left(\frac{d\sigma}{d\Omega}\right)_{\text{lab}} \right\rangle = \frac{1}{4\pi} \int_0^{\pi} d\Theta_{\mathbf{R}} \sin\Theta_{\mathbf{R}} \times \int_0^{2\pi} d\Phi_{\mathbf{R}} \left(\frac{d\sigma(\mathbf{R})}{d\Omega}\right)_{\text{lab}} . \quad (23)$$

The integrals were found to be accurately evaluated using an extended Simpson's $\frac{3}{8}$ rule for the specific angular values employed of $\Theta_{\mathbf{R}} = [0°(15°)180°]$ and $\Phi_{\mathbf{R}} = [0°(30°)180°]$ with $R = R_e$. The symmetry of the amplitude for $\Theta_{\mathbf{R}} \to 180° - \Theta_{\mathbf{R}}$ and $\Phi_{\mathbf{R}} \to 180° + \Phi_{\mathbf{R}}$ allows the sum over $\Phi_{\mathbf{R}}$ to go only up to 180°. The total number of points used in the sum is $7 \times 13 = 91$. Generally, an additional nonuniform averaging may be performed based on the particular vibrational- and rotational-state occupations.

For protons incident at 10 MeV, Fig. 8 shows the differential capture cross sections obtained using the B2-LPA with the HF wave function averaged over all calculated $\hat{\mathbf{R}}$ angles as in Eq. (23) or using the HF B2-LPA for $\Theta_{\mathbf{R}} = 0°$, $\Phi_{\mathbf{R}} = 0°$ or using the approximate B2-LPA averaged over angles. Also, the B2-LPA results for protons on hydrogen atoms, multiplied by a factor 2.67 to account for the different Laboratory-frame transformation factors, are shown. Remarkably, this figure shows that the averaged cross section differs relatively little from the one for the molecule along the incident direction, the former being at most 30% smaller in the forward direction. It is surprising that the angular averaging does not broaden or diminish the height of the Thomas peak. The position of the averaged approximate B2-LPA curve relative to the full curve is similar to that seen for the molecule along the incident direction, but, here, they tend to agree in the forward direction. Interestingly, there is an extra dip in the averaged HF and approximate B2-LPA cross sections just before the Thomas peak. The origin of this feature is not known, but it is apparently not entirely an artifact of the approximate evaluation. The averaged molecular and atomic cross sections are similar in shape, but the atomic one is a factor 2 lower in the forward direction and some 30% lower at the Thomas peak. Also, the minimum in the atomic case is not nearly as deep. The shape of the averaged approximate B2-LPA curve is very close to that of the atomic curve, which is not too unexpected since the molecular amplitude Eq. (21) contains the atomic one, but the molecular effective charge is 1.1, instead of 1. A final point is the more pronounced Thomas peak behavior in the molecular case.

For protons incident at 2.5 MeV, Fig. 9 presents the differential capture cross sections obtained using the same approximations as for those shown in Fig. 8. In this figure, the shapes of the two curves are very close, but the averaged cross section differs considerably more in magnitude from the one for the molecule along the incident direction than was seen in Fig. 8; the averaged curve is about 40% smaller in the forward direction and 30% smaller at the Thomas peak. The position of the averaged approximate B2-LPA curve relative to the full B2-LPA curve is similar to what was seen for the molecule along the incident direction, but the two tend, again, to agree in the forward direction. The atomic and averaged molecular cross sections at this lower energy are now of rather different shapes, with the former not hav-

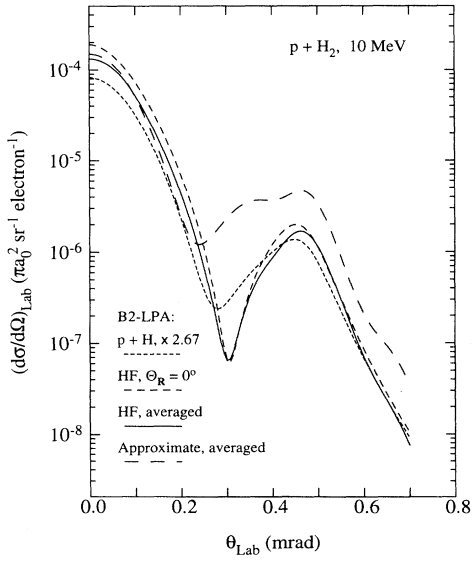

FIG. 8. For protons incident at 10 MeV on hydrogen molecules, differential capture cross sections obtained using the B2-LPA with the HF wave function, averaged over all $\hat{\mathbf{R}}$ angles according to Eq. (23) or for $\Theta_{\mathbf{R}} = 0°$, $\Phi_{\mathbf{R}} = 0°$ alone, and using an approximate evaluation of the B2-LPA, Eq. (21), averaged over all angles; for protons on hydrogen atoms, cross sections obtained using the B2-LPA, multiplied times 2.67.

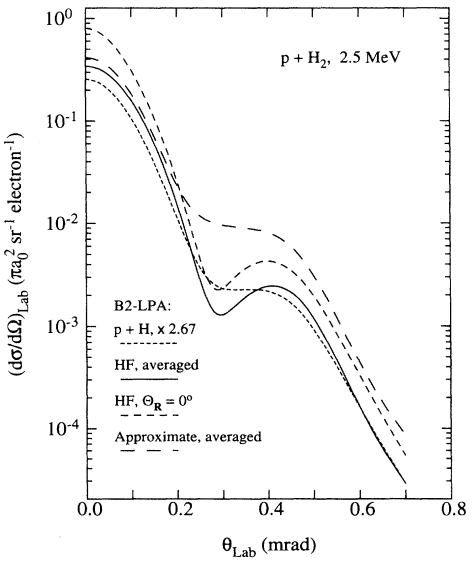

FIG. 9. For protons incident at 2.5 MeV on hydrogen molecules, differential capture cross sections obtained using the B2-LPA with the HF wave function, averaged over all $\hat{\mathbf{R}}$ angles according to Eq. (23) or for $\Theta_{\mathbf{R}} = 0°$, $\Phi_{\mathbf{R}} = 0°$ alone, and using an approximate evaluation of the B2-LPA, Eq. (21), averaged over all angles; for protons on hydrogen atoms, cross sections obtained using the B2-LPA, multiplied times 2.67.

ing a Thomas peak, only a shoulder. The atomic curve is a factor of 2 smaller in the forward direction. At this energy also, the shape of the averaged approximate B2-LPA curve is very close to that of the atomic curve, though shifted upwards in the Thomas-peak region.

IV. CONCLUSION

In summary, it has been shown that a more pronounced Thomas peak is found in the molecular case, even after averaging over molecular orientations. The approximation considered which separates the double-scattering mechanism from the diffraction aspect of the capture event leads to an atomiclike cross section which is too high at the Thomas peak and which gives a very poor representation of the molecular cross section. The two aspects of the capture process cannot be separated. Diffraction effects (the existence of deep minima) are readily apparent in the cross sections for a majority of molecular orientations. The minima are mostly compensated by cross sections at other orientations. The cross section averaged over all orientations is found to be similar in shape and somewhat smaller in comparison with the one for the molecule oriented along the incident direction, at both 10 MeV and at 2.5 MeV.

ACKNOWLEDGMENTS

I thank T. G. Winter for help with the calculation of the amplitude for the rotated molecule, J. H. Macek for his hospitality while on sabbatical at UT, and G. Morris for help with the computer code. This work is supported by the U. S. Department of Energy, Office of Energy Research, Office of Basic Energy Sciences, Division of Chemical Sciences.

[1] L. H. Thomas, Proc. R. Soc. London Ser. A **114**, 561 (1927); R. Shakeshaft and L. Spruch, Rev. Mod. Phys. **51**, 369 (1979).
[2] R. M. Drisko, Ph.D. thesis, Carnegie Institute of Technology, 1955 (unpublished).
[3] J. S. Briggs and L. J. Dubé, J. Phys. B **13**, 771 (1980); L. J. Dubé and J. S. Briggs, *ibid.* **14**, 4595 (1981).
[4] S. Alston, Phys. Rev. A **38**, 6092 (1988).
[5] J. H. McGuire and P. R. Simony, J. Phys. B **14**, L737 (1988).
[6] K. Dettmann and G. Leibfried, Z. Phys. **218**, 1 (1969).
[7] T. F. Tuan and E. Gerjuoy, Phys. Rev. **117**, 756 (1960).
[8] S. Fraga and B. J. Ransil, J. Chem. Phys. **35**, 1967 (1961).
[9] G. Herzberg, *Molecular Spectra and Molecular Structure. Vol. I: Spectra of Diatomic Molecules* (Krieger, New York, 1989), p. 534.
[10] I. Ben Itzhak (private communication).
[11] S. Cheng (private communication).
[12] E. Horsdal-Pedersen, C. L. Cocke, and M. Stockli, Phys. Rev. Lett. **50**, 1910 (1983); H. Vogt, R. Schuch, E. Justiniano, M. Schulz, and W. Schwab, *ibid.* **57**, 2256 (1986).
[13] C. J. Joachain, *Quantum Collision Theory* (North-Holland, Amsterdam, 1975).
[14] G. E. Forsythe, M. A. Malcolm, and C. B. Moler, *Computer Methods for Mathematical Computations* (Prentice-Hall, Englewood Cliffs, 1977), Chap. 5.
[15] J. Macek and S. Alston, Phys. Rev. A **26**, 250 (1982).
[16] B. J. Ransil, Rev. Mod. Phys. **32**, 239, 245 (1960).
[17] Private communication from S. Weinbaum, in L. Pauling and E. B. Wilson, *Introduction to Quantum Mechanics* (Dover, New York, 1963), p. 347.